





SPECIAL ISSUE ARTICLE OPEN ACCESS

Towards Contactless Daylight Photoluminescence of PV Strings During Operation by Electrical Modulation

C. Terrados^{1,2} | D. González-Francés¹ | K. P. Sulca¹ | C. de Castro¹ | M. A. González¹ | O. Martínez¹ 📵

¹GdS-Optronlab Group, Dpto. Física de la Materia Condensada, Universidad de Valladolid, Valladolid, Spain | ²Solar and Wind Feasibility Technologies (SWIFT). Escuela Politécnica Superior, Universidad de Burgos, Burgos, Spain

Correspondence: O. Martínez (oscar.martinez@uva.es)

Received: 1 July 2024 | Revised: 10 May 2025 | Accepted: 2 June 2025

Funding: This work was supported by the Spanish Ministry of Science and Innovation, under projects (PID2020-113533RB-C33 and PID2023-148369OB-C4), Universidad de Valladolid, Ministerio de Trabajo y Economía Social, European Union NextGenerationEU, Banco de Santander, Ministerio de Ciencia e Innovación, and Junta de Castilla y León.

Keywords: daylight photoluminescence | noninvasive | on-site inspection | PV strings | solar cell defects

ABSTRACT

Daylight photoluminescence (dPL) has emerged in recent years as a useful tool for inspecting solar panels, allowing for the identification of various types of defects with good spatial resolution and is now considered a useful technique for on-site qualification of field-deployed PV modules. The advantage of dPL is that it does not require an electrical power source, although the switching between two states is generally necessary to filter the ambient light. Several practical solutions have been implemented to carry out this type of measurement. In this paper, we describe the method based on the fast electrical switching using an electronic device connected to a string or substring in such a way that allows it to be switched between two states, with different currents drawn from the panels. The inspection is carried out with the string in operation, which makes it easier to monitor the condition of the panels throughout the life of the installation. The advantage of this method is being able to switch—in a very fast and noninvasive manner—the state of the string, between the maximum power point state and a state at (or very close to) open circuit conditions, once the electrical device has been installed. A demonstrative test has been carried out on a substring of panels, testing the response of two different inverters, in addition to a demonstration (using a microinverter) related to inspecting a whole string. Changes in the currents drawn from the panels, the response of the inverter, the background filtering procedure, and the quality of the images obtained are discussed in detail. dPL measurements obtained using this procedure are compared with previous dPL measurements and with daylight electroluminescence (dEL) measurements in order to verify the information provided by this new procedure.

1 | Introduction

Photovoltaic (PV) energy has grown exponentially in recent years, surpassing 1 TW of global installed capacity in 2022, and is now growing at rates of 200 GW per year [1]. Monocrystalline silicon solar cells are mainly used for terrestrial PV due to the abundance of silicon dioxide, coupled with large reductions in production costs [2]. For instance, the global weighted-average levelized cost of electricity (LCOE) of

newly commissioned utility-scale solar PV projects fell from 0.445 to 0.049 US\$/kWh between 2010 and 2022—a decrease of 89% [3]. A medium-sized PV plant of 50 MW consists of hundreds of thousands of Si PV panels, which are the core elements that produce the electricity. Operation and maintenance (O&M) should include carefully monitoring for the presence of defects in the panels, which can be caused by installation and normal operation, but also by climatological conditions (such as hailstorms) or other types of events, and which will lead to

This is an open access article under the terms of the Creative Commons Attribution-NonCommercial License, which permits use, distribution and reproduction in any medium, provided the original work is properly cited and is not used for commercial purposes.

© 2025 The Author(s). Progress in Photovoltaics: Research and Applications published by John Wiley & Sons Ltd.

a drop in the power produced by the panels and thus a reduced productivity of the PV plant [4-7]. Common inspection techniques for defect characterization of Si solar panels include visual inspection, I-V characterization, infrared thermography (IRT), electroluminescence (EL), and UV fluorescence [8–10]. Considering the huge number of panels in a PV plant, IRT inspection with a drone is the most widely used technique for large-scale inspection, as it is performed during operation and only requires high irradiation conditions ($> 600 \,\mathrm{W/m^2}$) [9, 11]. However, the information obtained is poor due to the low spatial resolution when flying a drone far away from the panels, and because the information obtained (hot spots) is difficult to link to a specific defect. I-V characterization of complete strings can be performed, although the information obtained is again also limited and only major problems on the string can be detected [10], without any direct correlation to specific defects in the panels at the cell level. I-V characterization at the panel level is desirable but proves time-consuming and is often only performed on suspected degraded panels. In contrast, luminescence techniques (electroluminescence [EL] and photoluminescence [PL]) provide high spatial resolution and allow different types of defects to be detected [6, 9]. EL inspection specifically allows large amounts of information about different types of defects to be obtained (both at the material and cell level) [12], although it suffers from two major drawbacks: It has traditionally been performed with very high-resolution Si cameras, for which a strict dark environment is needed due to the very low quantum efficiency (QE) of these cameras in the IR range, and it also requires the injection of current into the panels/string, which necessitates a power supply, and usually the need to disconnect the panels from the inverter. EL inspection in total darkness (nEL) using Si cameras has traditionally been carried out as a standard inspection technique and is very well suited as an approval inspection technique before the Si solar panels are installed in a PV plant. nEL is also widely used to inspect the solar panels installed on a solar PV plant, although the strict dark conditions required when using Si cameras is a major drawback, since it requires working at night or disassembling the panels to be inspected in a laboratory or in a dark environment in a mobile van [13, 14]. For these reasons, nEL is usually performed only on a very reduced number of panels in the plant. On the other hand, PL imaging using lamp/LED light sources for excitation can also be used to obtain information about defects in solar cells [15], mainly at the laboratory scale. However, the need for a homogeneous illumination source makes the use of PL imaging for panel characterization not easy. Recently, on-site PL measurements have been developed using a LED [16, 17] or a laser diode [18] as the excitation source. For example, PL imaging can be performed at night using Si cameras (hence with very high resolution) with multiple LED excitation to ensure homogeneity, although this usually implies a very heavy system as well as the need to power the LEDs [16, 17]. On the other hand, PL imaging with laser diode excitation can be performed at low irradiance levels using an InGaAs camera, although it is not easy to guarantee the homogeneity of the illumination and a scanning system of the laser diode is also required [18]. In an effort to overcome these limitations, daylight EL (dEL) has been developed in recent years [19-23] and offers the possibility of inspecting panels on-site during the day, thereby affording clear advantages in terms of the inspection procedure

and thus the possibility of inspecting a much larger number of solar panels. This requires cameras with a high QE in the near IR range, as well as methods for filtering ambient light. The dEL image is usually obtained by subtracting the signal when the panel is powered ("on" state) from when the panel is not powered (open circuit conditions -OC, "off" state). With regard to daylight PL (dPL), the technique was also developed parallel to dEL and has the advantage of not needing a power source for excitation, as it uses the sun as a light excitation source [14, 23, 24]. In order to eliminate ambient light background, dPL still usually requires two states ("on" and "off") to distinguish light from the panels from ambient light. Since the luminescence coming from a solar cell is proportional to the exponential of the diode voltage (V_d) [25, 26], the "on" and "off" states are selected with a large difference in V_d, and thus in the current drawn from the solar cell. For this purpose, the "on" state should be one in which a small current is drawn from the panels—for example OC conditions—while the "off" state should be one in which a large current is drawn from the panels (e.g., short circuit [SC] or maximum power point [MPP] conditions). In the "on" state, the photogenerated carriers recombine radiatively, producing a luminescence signal. In the "off" state, most of the photogenerated carriers flow through the electrical circuit and the luminescence signal is reduced. The difference between the two states allows the PL signal to be extracted [23, 24]. dEL and dPL have been included in a recent technical review as highly convenient techniques for on-site qualification of field-deployed PV modules, allowing for the inspection of a large number of solar panels without the need to disassemble and transport the PV modules to a laboratory [27].

We previously developed a dEL/dPL procedure based on electrical switching between two states [23]. In particular, for the dPL method, the procedure consists of switching the panels between the OC ("on" state) and SC ("off" state) points of the I-V curve of the panel. To acquire the dPL image, we used an InGaAs camera, specific filters to filter as much ambient light as possible, and an electronic device that very quickly switches between the OC and SC states, and is also synchronized with the InGaAs camera to acquire the signal in both states (hereafter referred to as dPL_{OC/SC}). For the practical realization of the dPL measurements, the whole string was disconnected from the PV plant, and the individual Si panels were disconnected from the string. The electronic device was then connected to each of the individual panels. The electronic device itself acts as the electrical connection (charge) for the SC state. The method can also be scaled up to the whole string.

Various approaches have also been used to obtain the dPL image by switching the panels between two states in order to have a large difference in PL emission, for which purpose electrical or optical switching have been developed [25, 26]. In the case of optical switching, a LED with up to one sun equivalent intensity can be placed to cover a solar cell, to inspect one panel [24], or multiple optical modulators (LEDs) to inspect a whole string [28, 29]. When the LED is off, the solar cell is completely shaded, which changes the bias condition of all the other cells connected to the same bypass diode ("on" state). When the LED is on, the solar cell and the whole panel are operating normally ("off" state). In this case, although the system can be described

as contactless and optical switching can be very fast, the optical modulators have to be mounted on and removed from some of the solar cells/panels, which is still a somewhat contact operation. Various approaches to contactless electrical switching have also been developed in recent years, mainly by using the inverter to produce the change between two states. Some procedures use the I-V sweep performed by some inverters [30, 31], although this is not a fast method, and the operator does not have full control over the process, as it depends on the IV sweep time itself; moreover, the variations in external irradiance during the measurement process would be detrimental to image quality and are difficult to correct [31]. Other procedures force the inverter to change between two states, which is generally not a fast method either [32]. Very recently, new developments have involved modifying the inverter itself to produce the change between the two states quickly [25, 33]. This development has great potential as it can be used to inspect PV systems on a large scale [33] but cannot be used for installed plants that lack this capability in the inverters. It is also possible to carry out dPL measurements without the need for two operating points, but with the use of two different filters [34], or even directly with the use of just one ultranarrow filter centered at ~1135 nm [35]. The latter is a very interesting approach for a fully contactless dPL measurement, although it does evidence certain drawbacks-mainly the need to use long exposure times to obtain enough PL signal and to remain completely in front of the area being inspected.

In an attempt to achieve a noninvasive inspection method based on dPL that can be performed with very short acquisition times, with the whole string working normally and without the need to modify the inverter, we show a modification of our previous dPL method by electrical switching (dPL_{OC/SC}) [23], by using an electronic device to force a substring of S-N panels (of a whole string of S panels) to work at two different points on the I-V curve—hereafter referred to as $dPL_{S(N)}$. The method can also be applied to a whole string of S panels. In this case, one string (of p strings connected in parallel to an inverter) is forced by means of the electronic device to work at two different points of the I-V curve—hereafter referred to as dPLs. The method is completely contactless once the electronic device is installed and is very fast. Such a device is a very cheap element that can be installed easily in every string to be inspected and can be activated remotely.

This paper aims to show the realization and capabilities of the $\mathrm{dPL}_{\mathrm{S(N)}}/\mathrm{dPL}_{\mathrm{S}}$ methodology, focusing on changes in the current drawn from the panels, the response of the inverter, and the quality of the $\mathrm{dPL}_{\mathrm{S(N)}}/\mathrm{dPL}_{\mathrm{S}}$ images obtained, and to compare the results with our previous $\mathrm{dPL}_{\mathrm{OC/SC}}$ methodology as well as with dEL.

2 | Materials and Methods

We used an InGaAs camera, Hamamatsu C12741-03, with 640×512 pixels, 14 bits' resolution, pixel noise of 250 e-rms, and dark current of 360,000 e-/pixel.s. Exposure times range from 1 μ s to 1 s, which enables acquisition to be adapted to the different lighting conditions. A Kowa short-wave infrared (SWIR) optical system with 16-mm focal length was used for image acquisition. A SWIR bandpass filter—centered around 1160 nm

with a bandwidth of 150 nm and a transmittance close to 90%—is used.

The electronic device used to switch the polarization states consists of a 1700-V IGBT (IXGN100N170 model), which is sufficient for a complete string operating at 1500 V and carrying 10 A.

We tested two different inverters. Inverter 1 (hereafter referred to as INV1) is a SUN 3Play TL-20-kW Ingeteam inverter, with an operating range of 560–820 V. Inverter 2 (hereafter referred to as INV2) is a Fronius Symo 4.5–3-M model with a working range of 150–1000 V. We also used a microinverter (APS DS3 880W 230V model) capable of working with two panels in parallel, in order to demonstrate the method for inspecting whole strings in operation.

Probes were performed using a whole string of 20 modules (mc-Si, ND-AR 330W model from Sharp), with $V_{\rm OC}$ =45.5V, $I_{\rm SC}$ =9.4 A, $V_{\rm MPP}$ =37.1V, $I_{\rm MPP}$ =8.9 A (at STC) or just a string of 16 modules from the whole string. Two separated panels (mc-Si, GCL-P6/72H340 from GCL), with $V_{\rm OC}$ =46.6V, $I_{\rm SC}$ =9.49 A, $V_{\rm MPP}$ =38.2V, $I_{\rm MPP}$ =8.9 A (at STC), were also used for testing.

Effective voltage and current signals were also recorded using Fluke 80K-40 and Fluke 80i-110s probes, respectively. The current probe is easy to handle as it is a Hall bridge sensor probe that does not need to be wired into the junction, but simply clamped to the positive or negative wires of the photovoltaic set. A TBS1052B 2-channel oscilloscope with 50-MHz bandwidth was used to record the signals. The probes used are compatible with the oscilloscope's high input impedance of 1-M Ω |20 pF. Measurements are shown as 5-s time segments. Blanks correspond to the limitations of the oscilloscope, which are unavoidable when using this particular equipment. Effective voltage is displayed as a very noisy signal due to the fact that the reference terminal is placed on the earth terminal and not on the negative terminal of the solar panels. This is because the probe works with a high-impedance voltage divider, such that the circuit is short-circuited if it is connected to the positive and negative terminals of the panels.

The global plane-of-array irradiance (G) was measured in situ using a power meter, in the plane of the modules, just before and after image acquisition.

It should be noted that we take dPL (and dEL) images of PV modules that are tilted with respect to the perpendicular of the camera objective (a very common situation when inspecting PV modules on-site in the PV plants) and perform a perspective transformation to present the images in a planar form. As a result, the image of the most distant part of the module may have a lower resolution, causing this part of the image to appear blurred in some cases. (While image optimization is an important issue, our current focus in this work is on validating the methodology for daylight luminescence acquisition).

2.1 | Description of the Procedure

The contactless $dPL_{S(N)}/dPL_{S}$ procedure involves detecting the luminescence signal coming from the panels in two states ("on"

and "off") by means of very fast (millisecond times) electrical switching between them, which can be carried out because the time delay is controlled by the user. This fast switching modifies the electrical current drawn from the panels, while the voltage remains almost unchanged. The main motivation is to be

(a) Inverter

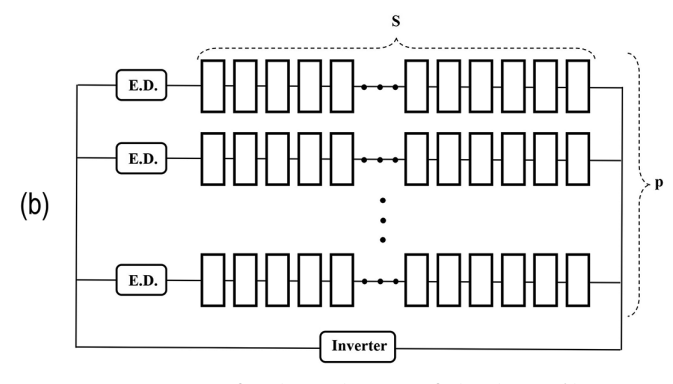


FIGURE 1 | Set-up for the realization of the $dPL_{S(N)}/dPL_S$ measurements. (a) For the $dPL_{S(N)}$ procedure, an electronic device (ED) is connected in parallel to the number N of panels to be isolated; (b) for the dPL_S procedure, in a configuration with p strings in parallel, the electronic device (ED) is connected in series with the string(s) to be inspected.

able to perform the measurements while the string is operating normally.

The main idea of this development is to make the dPL measurements as noninvasive as possible. Since an electronic device is used, the principal aim is to place it on a string and to control it remotely. Once installed, the electronic device could remain on the string for its whole life—if desired. All that is needed is a battery that can be connected to the electronic device when inspection is carried out and which is then removed. Remote activation of the electronic device is therefore the only operation required to inspect the string. To illustrate the principles of the method, a string of S panels is used, and the electronic device is connected in parallel to N modules of the string (Figure 1a). In this way, the substring of S-N panels can be inspected. It is also possible to inspect whole strings. For this purpose, in a configuration with p strings in parallel, the electronic device should be connected in series with the string(s) to be inspected (Figure 1b).

2.1.1 | Inspection of a Substring of S-N Panels

Let us consider a single string of S panels (each with $V_{\rm OC}$ and $V_{\rm MPP}$ values), connected to the maximum power point tracking (MPPT) of the inverter. The electronic device is connected in parallel with N panels of the string (Figure 1a) where N depends on the characteristics of the inverter, in particular its minimum operating voltage ($V^{\rm inv}_{\rm min}$), the total number of panels in the string (S), and the $V_{\rm OC}$ values of the panels as now described. The "off" state selected will be the one at the maximum power point (MPP), where the string normally operates, due to the MPPT function of the inverters, and therefore with a high current ($I_{\rm MPP}$) drawn from the panels (Figure 2a). This is the state when the electronic device is not activated. In order to obtain an "on" state, a point on the I-V curve with a higher voltage,

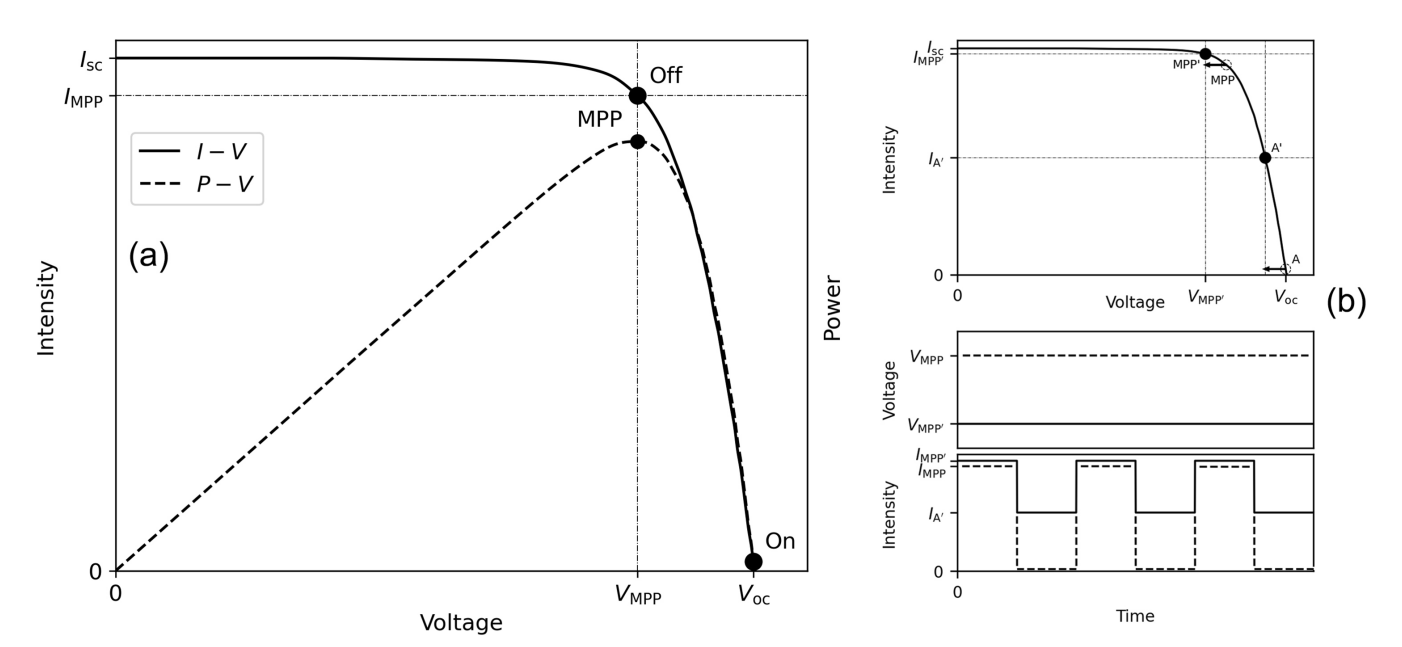


FIGURE 2 | (a) "On" and "off" states in the I-V curve used for the $dPL_{S(N)}$ (dPL_S) inspection of PV substrings (whole strings) during operation by electrical modulation. (b) Effect of the MPPT function to maximize power. The MPPT moves the point on the I-V curve a little to the left (lower voltage) to find new MPP' and A' points, where the power ($P=I\times V$) could be increased.

and therefore lower current drawn from the panels (ideally close to the OC conditions) is selected. In order to reach this state, the electronic device is now activated. Remote activation of the electronic device thus causes the N panels to become electrically isolated from the rest of the string, such that the inverter now only works with S-N panels. If the transition between the situation with S panels and that with S-N panels connected to the inverter is very fast, the inverter does not detect the very fast change, such that the rest of the string (S-N panels) will operate at the high voltage corresponding to the S panels— $S \times V_{MPP}$ which means that the operating point of the S-N panels moves to a higher voltage in the I-V curve, very close to V_{OC} if the number of panels (N) is properly selected, and therefore with a much lower current drawn from the panels than in the "off" state (see Figure 2a). As will be shown in Section 3, the inverter response really depends on the specific inverter model, which should be taken into account when carrying out these dPL_{S(N)} measurements.

According to the minimum voltage of the inverter (V^{inv}_{\min}) , the maximum number of panels (N) that can be electrically disconnected from the string of S panels, while maintaining the inverter operation, is given by

$$(S - N) \times V_{OC} \ge V_{min}^{inv}$$
 (1)

In this situation, if the inverter is not aware of the fast disconnection of N panels from the string, the S-N panels will not operate at $V_1 = V_{MPP}$ but at a higher voltage given by

$$V_2 = \frac{S}{S - N} \times V_{MPP} \tag{2}$$

This procedure is used in our method $(dPL_{S(N)})$ to switch the state of the S-N panels remotely (using a computer and wireless connection), thus between two points with a large difference in current intensities drawn from the panels ($I_{on} = I_{MPP}$, $I_{off} \sim 0$), and thereby obtaining two states with a large difference in luminescence signal intensity. This change is produced without forcing the inverter itself to switch between two states. Using the electronic device therefore makes it possible to achieve very fast switching, electrically connecting and disconnecting the N panels from the rest of the string. This allows a dPL image of the S-N panels to be obtained by subtracting the "on" and "off" signals, which are obtained at nearly the same external irradiation conditions (due to the very fast switching), thus favoring the quality of the obtained $dPL_{S(N)}$ image, and repeating the process as many times as required to filter ambient light as much as needed. By adequately selecting the number N, the V_{OC} condition can almost be reached for the S-N panels, with a large change in current drawn from the panels between the "off" and "on" states.

2.1.2 | Inspecting Whole Strings

The method can be extended to inspect an entire string in operation. In this case, for a configuration with p strings connected in parallel to the MPPT of the inverter, it is possible to connect the electronic device in series with the string(s) to be inspected. Here, the "off" state will again be the one at the MPP where the

p strings normally operate, and therefore with a high current (I_{MPP}) drawn from all the strings, and which is obtained in this case when the electronic device is activated. In order to obtain an "on" state, the electronic device is deactivated, thus disconnecting the string from the rest of the p strings -Figure 1bthereby forcing this string to work at OC conditions. Remotely disconnecting the string does not change the voltage in the MPPT of the inverter, while the change in the current drawn from the remaining p-1 strings connected to the MPPT of the inverter would be small, depending on the number (p) of strings connected in parallel to the inverter. This procedure is thus used to switch the state of the selected string remotely between two points with a large difference in current intensities drawn from the panels $(I_{on} = I_{MPP}, I_{off} = 0)$. Again, two states with a difference in the luminescence signal intensity are obtained, without forcing the inverter itself to switch between two states, where the "on" and "off" signals are collected at nearly the same external irradiation conditions (due to the very fast switching). This favors the quality of the dPLs image obtained, and the process may be repeated as many times as required to filter the ambient light as much as needed.

The main advantage of the explained procedures is that the electrical switching described here allows the dPL image of any of the panels of the substring $(dPL_{S(N)})$ or string (dPL_S) to be obtained, without the need to modify the inverter itself to force the required switching between two states. Very fast switching can be performed by controlling the electronic device with wireless communication, and the "on" and "off" time periods can be selected by the user, according to the solar irradiance conditions and the desired image quality. Here, we define the exposure times for acquiring the "on" and "off" luminescence images exactly the same as the "on" and "off" time periods, although exposure times can be shorter if required. As already mentioned, the electronic device is a very cheap element that can be installed in the strings that need inspecting, thereby making it easier to monitor the condition of the panels. The $dPL_{S(N)}/dPL_S$ procedure is thus contactless, which proves very beneficial when inspecting a large number of Si panels on-site at PV plants.

2.1.3 | Subtraction Procedure

The subtraction procedure used to obtain the dEL, $dPL_{OC/SC}$ or $dPL_{S(N)}/dPL_{S}$ images is the same. Only the points of the I-Vcurve ("on" and "off" states) for the different measurements are changed, as described above. This involves subtracting the ON signal vis-à-vis the OFF signal for each pixel, and accumulating the signal differences over a certain number of cycles (nc). Due to the presence of ambient light (background), the intensity signal (for both "on" and "off" periods) can be very large and may even saturate the sensor, while the ON-OFF signal difference can be very small. To avoid saturating the sensor, it is usual to play with the aperture of the camera objective. Exposure time (t_{exp}) can also be varied. For fast switching, t_{exp} is usually chosen in the range 3-12ms (the obtained images shown later were mainly obtained with $t_{exp} = 5 \,\text{ms}$), and the aperture is modified accordingly. On the other hand, for a fixed aperture value, a longer value of $t_{\rm exp}$ can be used at lower irradiances to increase the signal value. For the InGaAs camera used -with a resolution of 14 bits- the signal is limited to 16,384 gray levels (counts).

Our software is programed to store all the images, both for the "on" and "off" periods, for the nc cycles. 2 x nc images are thus obtained. The software is also programed to make the difference $\operatorname{Signal}_{(1)}^k = \operatorname{ON}_{(1)}^k - \operatorname{OFF}_{(1)}^k$ for each pixel k, store it as $\operatorname{Signal}_{(\operatorname{accum},1)}^k$, and then make the difference $\operatorname{Signal}_{(2)}^k = \operatorname{ON}_{(2)}^k$ -OFF(2) and add it to the previous accumulated value (Sig $\operatorname{nal}_{(\operatorname{accum},2)}^{(2)}{}^k = \operatorname{Signal}_{(\operatorname{accum},1)}{}^k + \operatorname{Signal}_{(2)}{}^k)$, and so on. A final image is obtained with the final $\operatorname{Signal}_{(\operatorname{accum},nc)}{}^k$ over the nc cycles for all the pixels, giving the resulting dEL or dPL image. Due to the noise and the effect of the background light, $Signal_{(m)}{}^k$ might become negative for a given cycle $nc_{(m)}$ on pixel k, which has no physical meaning. If that is the case, the cycle nc_(m) is not taken into account for that particular pixel when obtaining the final image. It should be noted that it is not necessary to store all the images if the signal-to-noise ratio (SNR) is not calculated. In such a case, only the final Signal (accum no) over the nc cycles for all the pixels would be collected, which is very convenient for inspecting a large number of modules (due to the difficulty of dealing with a large number of images).

In order to quantify the quality of the images obtained, the SNR was calculated from the $2\times$ nc partial images, according to the expression given in [29]:

$$SNR_{avg} = \frac{\sum_{k} \left[avg_{m \in 2xnc} \left(ON_{m}^{k} - OFF_{m}^{k} \right) \right]}{\sum_{k} \left| avg_{i \in n_{1}} \left(ON_{i}^{k} \right) - avg_{j \in n_{2}} \left(ON_{j}^{k} \right) \right| \cdot \sqrt{0.5} \left(\frac{2}{\pi} \right)^{-0.5} \right|}$$
(3)

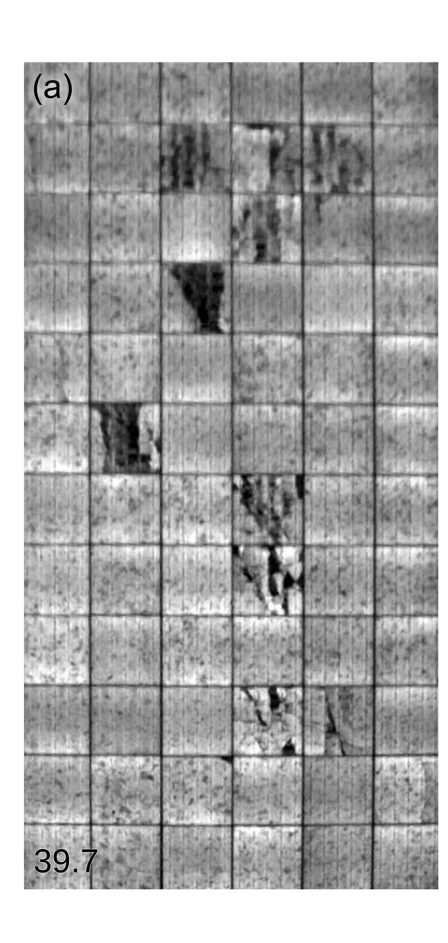
where n_1 represents the odd numbers between 1 and $2\times$ nc, and n_2 the even ones. SNR_{avg} is related to the signal-to-noise ratio SNR_{50} defined in [36]. For high irradiance conditions, the differences $Signal_{(m)}{}^k = ON_{(m)}{}^k - OFF_{(m)}{}^k$ can be as low as just a few tens of counts.

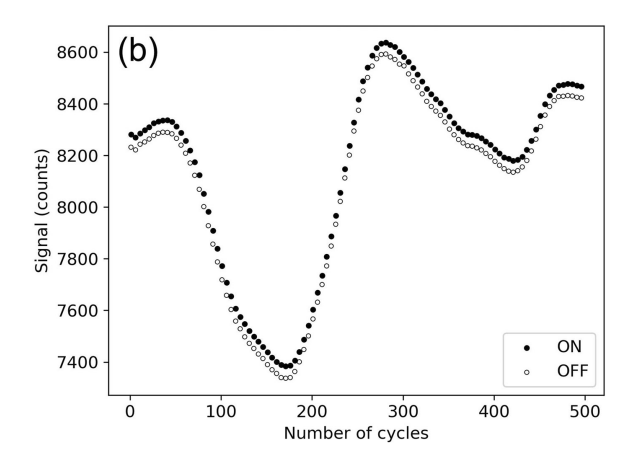
The SNR $_{\rm avg}$ is expected to decrease as the irradiance increases, because the background noise increases. In the case of the dEL images, the SNR $_{\rm avg}$ increases as a function of the current intensity injected into the panels by the power supply. In the case of the dPL images, the SNR $_{\rm avg}$ is expected to increase as the current difference drawn from the panels in the two selected states (ΔI) increases. In all cases, the SNR $_{\rm avg}$ should increase as the number of cycles increases.

3 | Results and Discussion

3.1 | Reference Images

In order to have reference images with which to compare, dEL and dPL $_{\rm OC/SC}$ images were obtained for a selected panel of the string used—which has some clear defects. Figure 3a shows the dEL image obtained for the case of G=1000 W/m², $I_{\rm current}$ =9 A, $t_{\rm exp}$ =5 ms, nc=500. The information provided by the dEL image is good enough to allow the defects present in the different cells of the panel to be clearly distinguished (the upper part





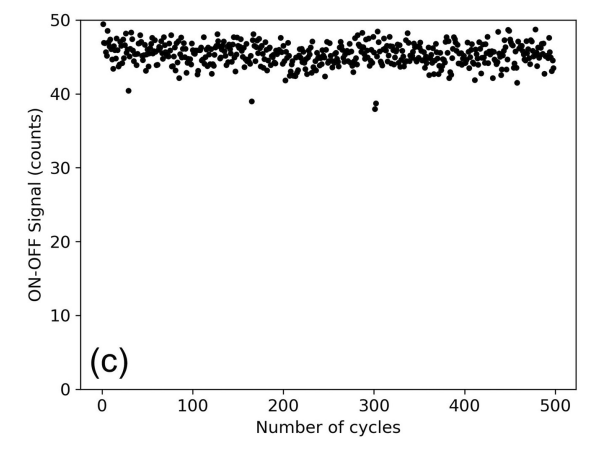


FIGURE 3 | (a) dEL image of a defective panel of the inspected string (I = 9 A, $G = 1000 W/m^2$, $t_{exp} = 5 ms$, nc = 500); (b) on and off signals (sum of the signal from all the pixels of the image) and (c) ON—OFF signal differences, both as a function of the number of cycles.

of the image is blurred because the PV panel is tilted with respect to the perpendicular of the camera objective). Figure 3b shows the signals (sum of the signal from all the pixels of the image) of both the "on" and "off" partial images, and Figure 3c shows the ON-OFF signal differences, both as a function of the number of cycles. Two important points should be emphasized: (i) The background signal can vary greatly: in this case there is a variation of 1300 counts over 8600 counts, that is, ~15% of the signal (Figure 3b); and (ii) the very small luminescence coming from the panel itself—only ~45 counts in this case (Figure 3c). In spite of the very small ON-OFF signal differences, the SNR_{avg} value (indicated in the left bottom side of the images), which is calculated from Equation (3), is 39.7 for this measurement (nc = 500). According to refs. [36, 37], a value above five can be considered sufficient for outdoor EL. As emphasized previously [38], the nEL image obtained also with the InGaAs camera gives nearly the same visual information on the defective areas as the information provided by the dEL image (see Figure S1). The proper observation of the defects is limited by the resolution of the InGaAs camera used, not by the ambient light filtering procedure. The nEL image obtained with a 12 MPx Si camera (see also Figure S1) obviously gives clearer information about the defects, due to the much higher resolution. Since the daylight inspection is only possible with a camera with a high QE in the IR, such as an InGaAs camera, the resolution of the InGaAs camera is currently a limiting factor. In any case, the dEL image allows to observe the main defects of the solar cells, which for this panel correspond to material imperfections (observed in all

the cells), cracks and microcracks, and areas with different degrees of electrical isolation (10 solar cells are largely affected). The low resolution of the InGaAs camera makes it difficult to see the microcracks in great detail.

Figure 4a shows the dPL $_{\rm OC/SC}$ image obtained for the same panel, for $G = 1000 \text{ W/m}^2$, $t_{exp} = 5 \text{ ms}$, nc = 500. Figure 4b shows the signals of both the "on" and "off" partial images, and Figure 4c shows the ON-OFF signal differences as a function of the number of cycles. As can be seen in Figure 4c, the signal differences are lower (~25 counts), and the data dispersion is much larger than those obtained in the dEL measurement acquired under the same conditions (Figure 3c). An SNR_{avg} value of 7.7 is obtained in this case. We attribute the large decrease in the SNR_{avg} to the fact that the luminescence signal is expected to be lower in dPL than in dEL, since in the dEL case the current injection provides the carriers needed to produce a luminescence signal (and taking into account that Si is an indirect bandgap material). Despite this, the dPL image still shows material imperfections and cells with dark areas. The same 10 defective cells are detected as in the dEL image, although the information provided by the dPL image is different and details of the severity of the defects are largely lost. In a recent paper we have discussed these differences in relation to the degree of isolation of the defective areas for cracked regions [38]. The information provided by the dPL technique has also been discussed in some papers [26, 35] and is recognized as still limited [26, 39]. Although the two techniques may not provide the same information, we observe

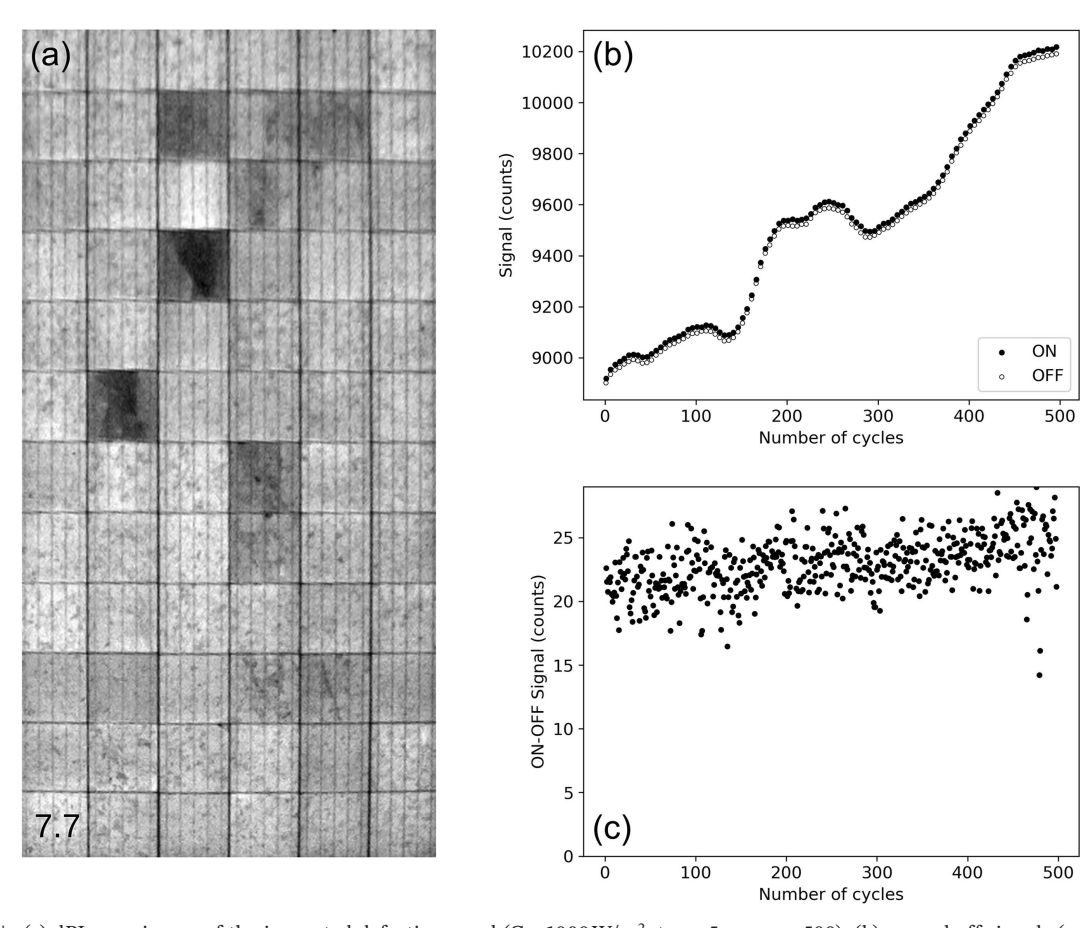


FIGURE 4 | (a) $dPL_{OC/SC}$ image of the inspected defective panel ($G = 1000 \text{ W/m}^2$, $t_{exp} = 5 \text{ ms}$, nc = 500); (b) on and off signals (sum of the signal from all the pixels of the image) and (c) ON—OFF signal differences, both as a function of the number of cycles.

that the defective cells are distinguished in both cases. Due to the advantage of not needing a power source for the dPL case, it can be advantageous in many cases to inspect the solar panels using the dPL technique rather than the dEL technique, as mentioned above.

3.2 | Inspection of a Substring of S-N Panels

For the practical implementation of the $dPL_{S(N)}$ procedure described above, two different inverters and a string with 20 or 16 mc-Si panels were tested. As will be shown, the Ingeteam model used (labelled as INV1) gives current intensity values for the "on" and "off" states almost constant, while the Fronius model used (labelled as INV2) shows large variations in the current intensity values.

3.2.1 | Inverter 1 and String With S = 20 Panels

As previously described, the mc-Si panels tested have V_{OC} and V_{MPP} values (at STC) of 45.5 V and 37.1 V, respectively. INV1 has a minimum operating voltage of 560 V. Using the entire string of S = 20 panels—and according to Equation (1)—the maximum number of panels that can be electrically disconnected while the inverter is still working (i.e., operating at voltages over 560 V) is seven, although this calculation has been made using the values given for STC, that is, for an irradiance G of 1000 W/m² and 25°C. According to Equation (2), each of the S-N panels (for S=20) will operate at a voltage of 57.1, 53, 49.5, 46.4, or 43.6 V, when N=7, 6, 5, 4, or 3, respectively, where the values have again been calculated for STC. These figures may vary slightly depending on the external irradiance and temperature conditions.

Figure 5 shows the $dPL_{S(N)}$ images obtained with our procedure (S=20) with the electronic device in parallel with 6 (a), 5 (b),

4 (c), and 3 (d) panels, for $G=1020\,\mathrm{W/m^2}$ and an external temperature of $10^\circ\mathrm{C}$. A $t_\mathrm{exp}=5\,\mathrm{ms}$ and nc=300 on/off cycles were used in all cases. Figure 5e-h shows the corresponding ON-OFF signal differences as a function of the number of cycles. Intensity and voltage variations—measured at the output of the inverter—are also shown in Figure 6a-d. As can be seen, a good square wave modulation is obtained for the current intensity in all cases, while the voltage (that of the inverter)—which is modulated according to the electrical grid value—does not show very significant changes. The maximum values of the current intensity ("off" periods) are constant (~8 A) in all cases, corresponding to the high irradiation conditions of the measurement ($I_{\mathrm{MPP}}=8.9\,\mathrm{A}$ at STC).

For N=6, the minimum current intensity value ("on" periods) is close to zero and is maintained over time for the whole measurement period (Figure 6a). The average effective voltage measured, which should correspond to the operating voltage of the inverter, is nearly maintained at around 620 V. As indicated—and according to Equation (2)—in this situation, each of the 14 panels would operate at ~53 V (at STC), which is much higher than the V_{OC} value (45.5 V). This in fact means that the panels are forced to operate in OC conditions, and therefore with almost zero current intensity. The $dPL_{S(N)}$ image obtained (Figure 5a) is of good enough quality (SNR_{avg} = 7.7) to clearly distinguish the defective cells (see Figure 3a and Figure 4a). As shown by the current and voltage measurements obtained with the probes used, this is due to the large difference in current intensity values between the "on" and "off" periods ($\Delta I \sim 8 A$), the fast switching between the two periods, and the perfect square modulation. In fact, it can be clearly seen that the mean ON-OFF signal differences are fully constant for this case (Figure 5e).

For N=5 (Figure 5b,f) and (Figure 6b), the quality of the $dPL_{S(N)}$ image obtained is also good enough ($SNR_{avg}=6.8$), again due to the large difference in the current intensities, fast

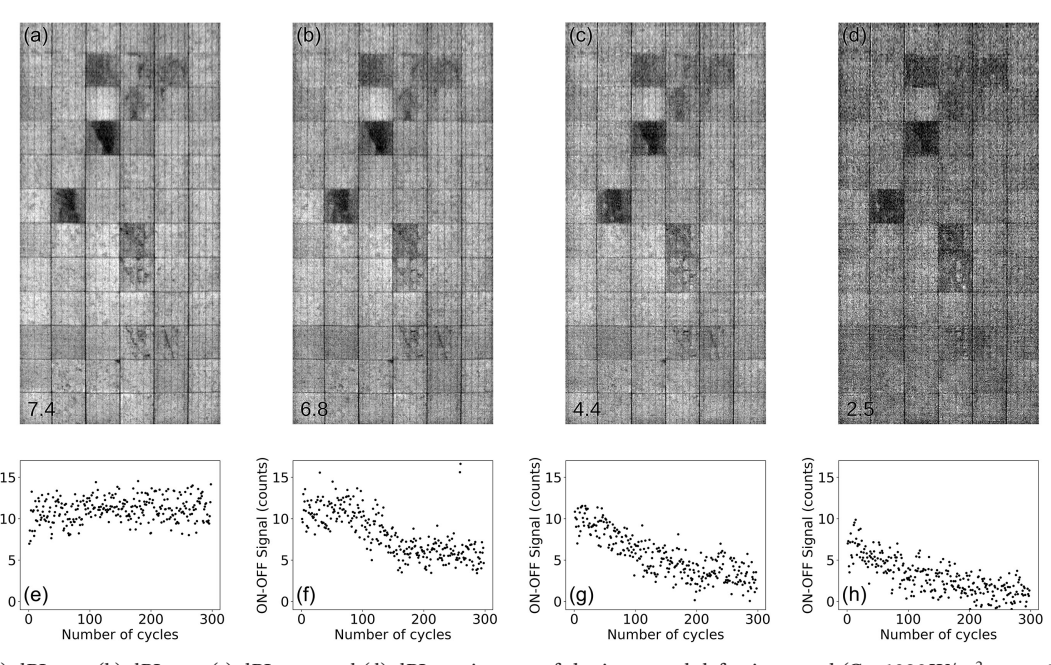


FIGURE 5 | (a) $dPL_{20(6)}$, (b) $dPL_{20(5)}$, (c) $dPL_{20(4)}$, and (d) $dPL_{20(3)}$ images of the inspected defective panel (G=1020 W/m², t_{exp} =5 ms, nc=300); (e-h) ON—OFF signal differences, as a function of the number of cycles: (e) 20/6, (f) 20/5, (g) 20/4, and (h) 20/3.

ON-OFF Signal (counts

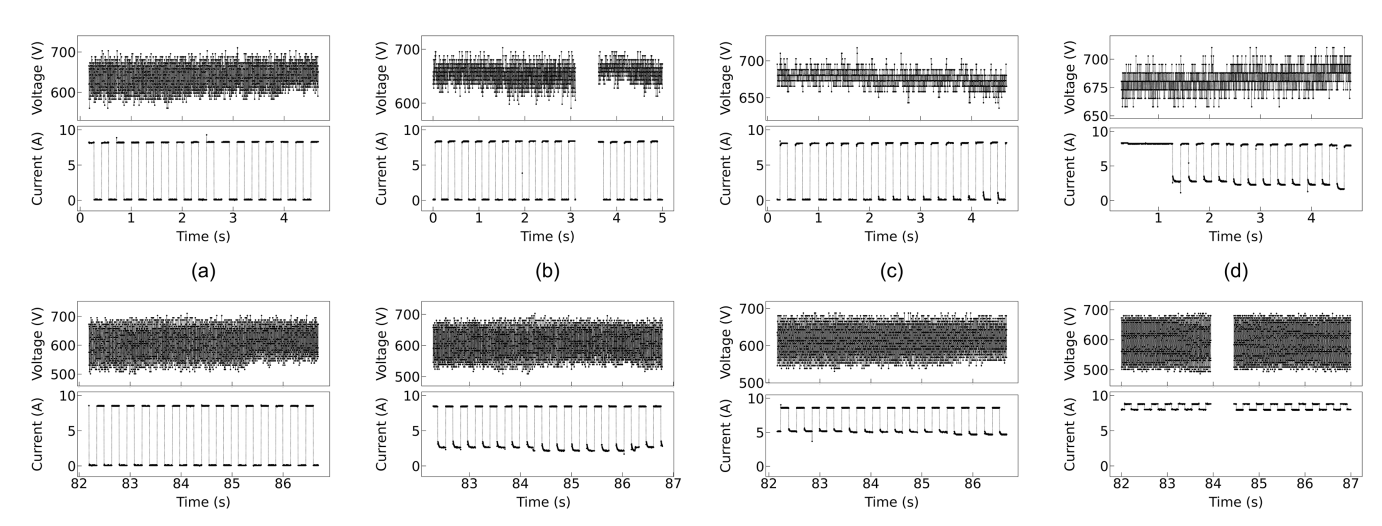


FIGURE 6 | Voltage and current intensity values, measured at the inverter, for situations displayed in Figure 5: (a) 20/6, (b) 20/5, (c) 20/4, and (d) 20/3; for each case, the two graphs represent the measured values for the first and last 5-s time segments, respectively.

switching and the almost perfect square shape. However, the minimum current is not constantly fixed at zero, as can be clearly seen at the end of the measurement period (Figure 6b). The minimum current value starts at zero and remains there for a few seconds, but then starts to increase. Furthermore, the average voltage has an initial value of ~660 V, while the final voltage measured is ~600 V. As expected—and according to Equation (2)—each of the 15 panels in this situation would operate at ~49.5 V, which is still higher than the V_{OC} value (45.5 V), such that the panels are expected to operate in OC conditions, and therefore with almost zero current intensity. However, the fact that the minimum current intensity is seen to increase from zero over time, together with the decrease in the mean inverter effective voltage from ~660 to ~600 V along the switching measurement process, is interpreted as the self-readjustment of the MPPT of the inverter to increase the maximum power. In fact, the inverter's MPPT is working constantly to find the maximum power. To do this, the inverters are usually programed to move the operating point to either side of the I-V curve. If the MPPT moves the point a little to the left (lower voltage) during the dPL_{S(N)} measurement, it could find new MPP' and A' points where the power would be increased, see Figure 2b. (It is important to note that during the switching process, the power would be that of the "on" periods plus that of the "off" periods.) As a result, the minimum current intensity would increase from zero (a small increase in the maximum current intensity would also be expected). In such case, the difference in current intensities drawn from the panels would not be constant during the measurement period, and the perfect square shape would not be maintained. This seems to be the case here, when five panels are electrically isolated from the string, resulting in a slightly lower quality (SNR_{avg}) dPL₂₀₍₅₎ image compared to the dPL₂₀₍₆₎ image. In fact, as can be seen in Figure 5f, there is a period of time (during measurement) when the mean ON-OFF signal differences have a relatively large value and are constant. However, after a while, the mean ON-OFF signal differences start to decrease and finally reach a new small value.

As the number N decreases further—N=4—the quality of the dPL image obtained decreases further (Figure 5c,g)

 $(SNR_{avg} = 4.4)$. This is due to the large minimum current intensity value of the On periods, which moves further away from zero as the number N decreases. It is again interesting to note that the initial value of the minimum current intensity is still zero for some seconds and then starts to increase (Figure 6c). In this case—and according to Equation (2)—each of the 16 panels would be working at ~46.4V in this situation, which is now very close to the V_{OC} value (45.5 V). This explains why the initial minimum current intensity is still zero. However, it increases to a final value of ~5.0 A, together with the fact that the average voltage of the inverter changes from an initial value of ~675 V to a final value of ~620 V. Again, these changes are interpreted as the self-readjustment of the MPPT of the inverter to increase maximum power (Figure 2b). The smaller difference in current intensities between the "on" and "off" states is detrimental to obtaining a good $dPL_{S(N)}$ image. As can be seen in Figure 5g, the mean ON-OFF signal differences have a relatively large initial value that immediately starts to decrease and finally reaches a low value.

For N=3, the quality of the $dPL_{S(N)}$ image is greatly reduced compared to the previous cases ($SNR_{avg} = 2.5$). As can be seen in Figure 6d, the minimum current intensity in this case does not start at zero, but at ~3.5 A and increases until reaching a value of ~7.5 A (the maximum current intensity also increases slightly which, as indicated, should be attributed to the slight increase in the maximum current intensity due to the self-readjustment of the inverter, Figure 2b). Figure S2 shows detailed changes in current and voltage (the mean calculated power is also shown) throughout the measurement period. In fact, according to Equation (2), in this situation, each of the 17 panels would operate at ~43.6 V, which is now lower than the $V_{\rm OC}$ value (45.5 V). In this case, we therefore have a small or very small current difference ΔI between the two states, with a square shape that is not perfect due to changes over time. Since the final $dPL_{S(N)}$ image is obtained by accumulating the image differences over the entire period of 300 cycles, the quality of the final image is much worse compared to the previous cases. Figure 5h shows the ON-OFF signal differences, where a relatively low initial value can be seen that immediately starts also to decrease, reaching a very small final value.

The experimental results obtained—as shown in Figures 5 and 6 (and Figure S2)—are in good agreement with the above description of the $dPL_{S(N)}$ procedure. For this string of S=20 panels, the optimum number of panels to be electrically disconnected is 6, since—as seen—the current square wave shape is perfectly

defined, with the minimum current value equal to 0 and constant throughout the measurement period. This is due to the large difference in the operating voltage compared to the $V_{\rm OC}$ value (self-readjusting of the MPPT of the inverter to increase the maximum power therefore has no effect). As the number N of

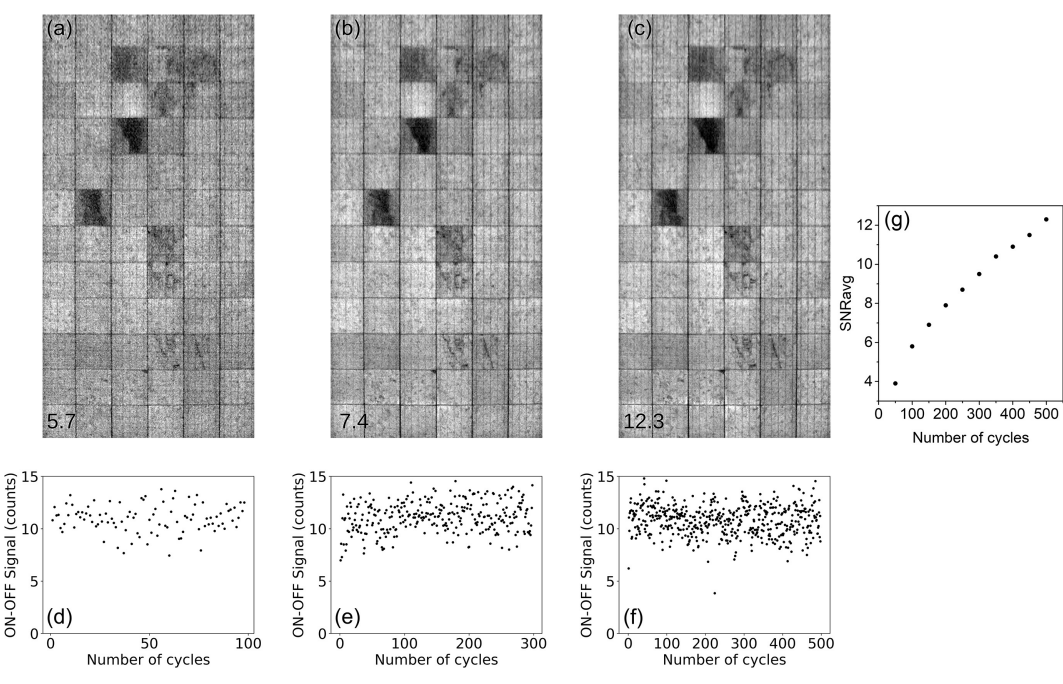


FIGURE 7 | dPL $_{20(6)}$ images of the inspected defective panel (G = 1020 W/m², $t_{exp} = 5$ ms) for different numbers of cycles: (a) nc = 100, (b) nc = 300, (c) nc = 500. (d-f) Corresponding ON—OFF signal differences, as a function of the number of cycles: (d) nc = 100, (e) nc = 300, and (f) nc = 500. (g) SNR $_{avg}$ as a function of nc (in this case, the original stack of 500 cycles was used, gradually eliminating a higher number of stacks).

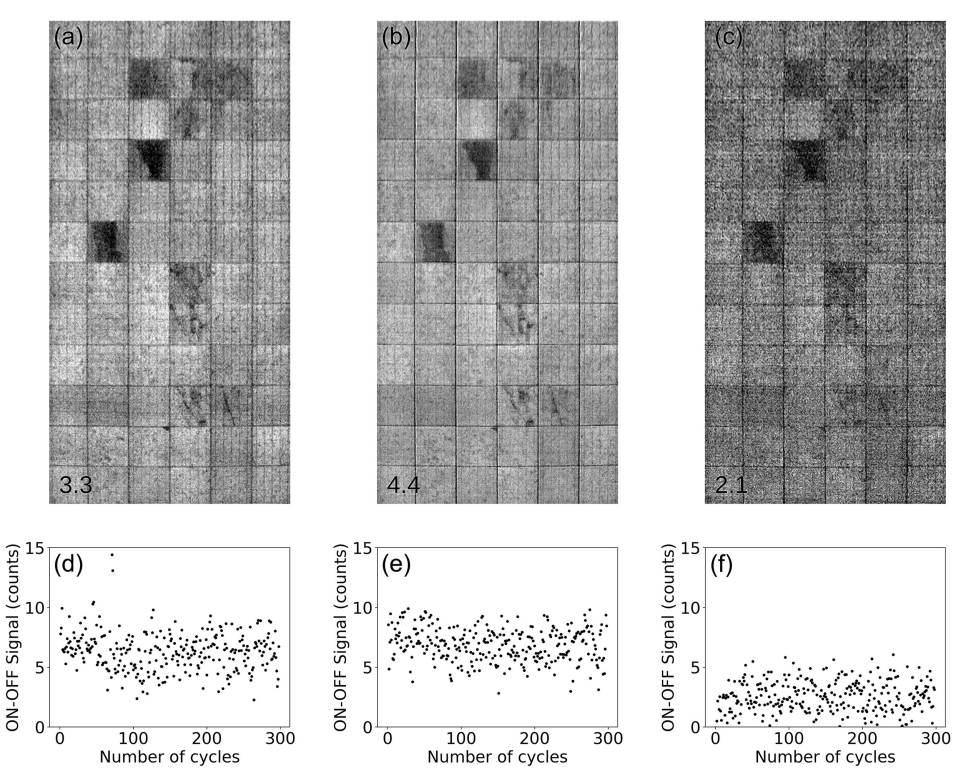


FIGURE 8 | (a) $dPL_{16(3)}$, (b) $dPL_{16(2)}$, and (c) $dPL_{16(1)}$ images of the inspected defective panel ($t_{exp} = 5 \, ms$, nc = 300, the irradiance G value fluctuates around $700 \, W/m^2$); (d-f) ON—OFF signal differences as a function of the number of cycles: (d) 16/3, (e)16/2, and (f) 16/1.

electrically disconnected panels decreases, the "on" state is still close to the OC state, but with a smaller difference in the operating voltage compared to the $\rm V_{OC}$ value. Self-readjustment of the MPPT of the inverter to increase maximum power produces an

increase in the minimum current intensity over time throughout the measurement period (Figure 2b). Although the quality (SNR $_{\rm avg}$) of the ${\rm dPL}_{\rm S(N)}$ image deteriorates as the number N of disconnected panels decreases from the optimum situation, the

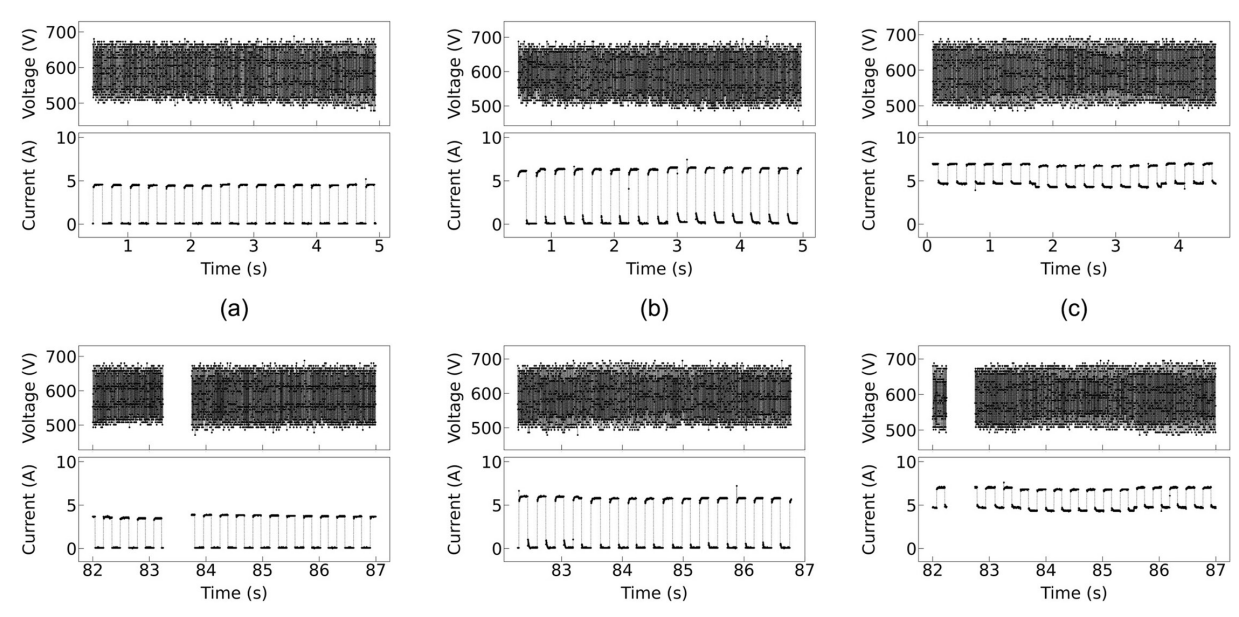


FIGURE 9 Voltage and current intensity values, measured at the inverter, for situations displayed in Figure 8: (a) 16/3, (b) 16/2, and (c) 16/1; for each case, the two graphs represent the measured values for the first and last 5-s time segments, respectively.

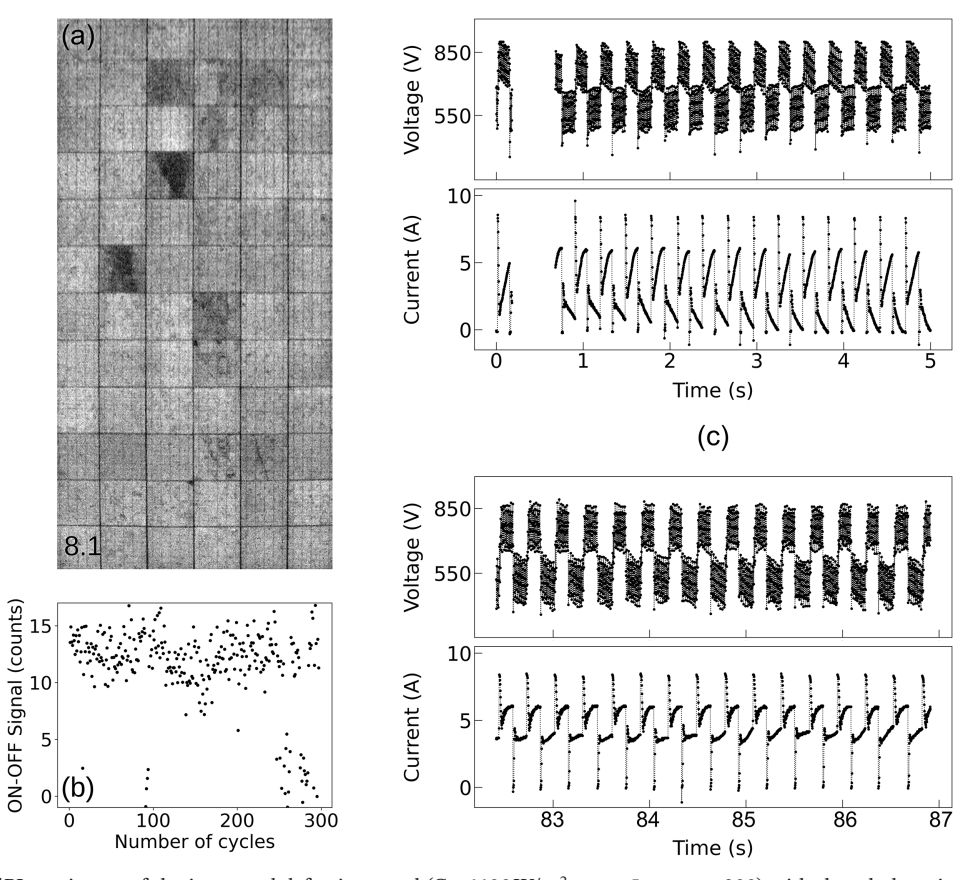


FIGURE 10 | (a) dPL $_{20(6)}$ image of the inspected defective panel (G=1100 W/m², $t_{\rm exp}$ =5 ms, nc=300) with the whole string connected to INV2; (b) ON—OFF signal differences as a function of the number of cycles and (c) voltage and current intensity values, measured at the inverter (the two graphs represent the measured values for the first and last 5-s time segments, respectively).

decrease is not so harmful and, for example, the 20/4 situation still gives a dPL image that allows the 10 defective cells with dark areas to be identified.

Figure 7 shows the $dPL_{20(6)}$ results for the case of G = 1020 W/ m^2 , $t_{eyn} = 5$ ms, varying the number of cycles (nc): 100 (a), 300 (b), and 500 (c). As expected, the image quality increases with the number of cycles, with SNR_{avg} values of 5.7, 7.4, and 12.3, respectively. Figure 7d-f shows the ON-OFF signal differences as a function of the number of cycles. The mean differences are constant and have approximately the same value regardless of the number of cycles. The improvement in the quality of the $dPL_{S(N)}$ image with nc is the result of accumulating a higher number of "on"/"off" differences and is how ambient noise is best eliminated, although it does imply longer inspection times. Figure 7g shows the variation of ${\rm SNR}_{\rm avg}$ as a function of nc. (To obtain this figure we calculated the $\tilde{\text{SNR}}_{\text{avg}}$ for the case of the original stack of 500 cycles and gradually eliminated a higher number of stacks and recalculated the SNR_{avg} value.) The aforementioned increase with nc can be observed, with a tendency to stabilize at large nc values. The total accumulation time of these measurements is ~90, ~130 and ~220 s, for 100, 300, and 500 cycles, respectively. It is important to note that this is our synchronous solution for obtaining daylight luminescence images [23] which, as explained, involves accumulating all the differences to obtain the final image synchronously; that is, acquiring the partial images synchronously with the "on" and "off" states. Total acquisition times are large due mainly to the limited maximum frame rate of the camera (60 fps). We have started to work with an asynchronous solution using a faster speed camera (maximum frame rate of 600 fps), which has initially provided quite good results in much shorter times [40]. Further work is in progress and will be published soon.

It is also interesting to note that the $dPL_{20(6)}$ image shown in Figure 7c resembles more the dEL image (Figure 3a) than the $dPL_{OC/SC}$ one (Figure 4a). We will comment on this point later on when discussing the dPL_{S} procedure.

3.2.2 | Inverter 1 and String With S=16 Panels

In order to evaluate the influence of the number of panels in the string on the $dPL_{S(N)}$ measurements, a string with S=16 panels was selected from the full string of 20 panels. In this case—and according to Equation (1)—the maximum number of panels that can be disconnected is N=3, although it can also be N=4, depending on ambient temperature. In this case—according to Equation (2)—each of the S-N panels (for S=16) will operate at a voltage of 49.5, 45.6, 42.4, or 39.6 V, when N=4, 3, 2, or 1, respectively, where again these values have been calculated for STC.

Figure 8 shows the $dPL_{S(N)}$ images obtained for this string of S=16 panels, for N=3 (a), 2 (b), and 1 (c) panels electrically isolated from the string, for nc=300 and $t_{exp}=5 \, ms$ in all cases. Figure 8d-f shows the ON-OFF signal differences

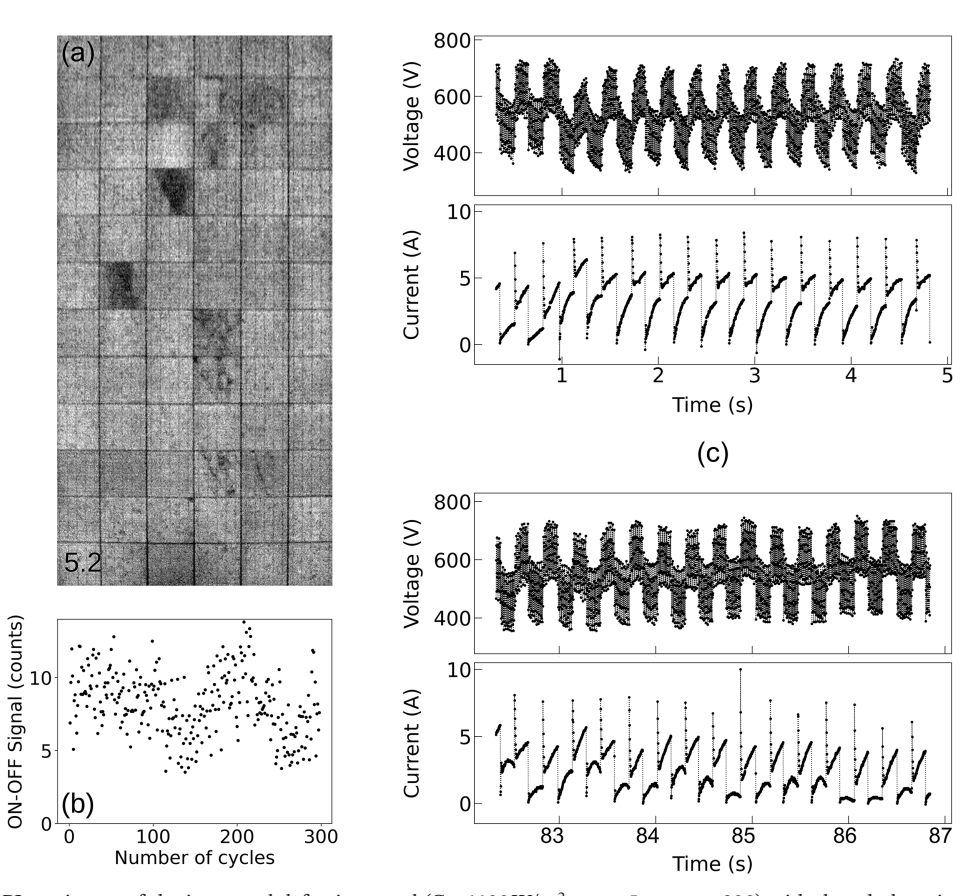


FIGURE 11 | (a) dPL $_{16(3)}$ image of the inspected defective panel (G=1100 W/m 2 , t $_{\rm exp}$ =5 ms, nc=300) with the whole string connected to INV2; (b) ON—OFF signal differences as a function of the number of cycles and (c) voltage and current intensity values, measured at the inverter (the two graphs represent the measured values for the first and last 5-s time segments, respectively).

as a function of the number of cycles. Irradiance conditions were not constant for this series, with G values around 700 W/ m², or higher in some cases. This can be deduced from the maximum current intensities measured (Figure 9a-c). As observed, almost perfect square wave shapes of current intensity are observed for N=3 and 2, with a minimum current intensity equal to 0 in both cases. The minimum current intensity value is much higher for the case N=1. As can be seen in Figures 8d-f, the mean ON-OFF signal differences are now approximately constant over the measurement period (they are lower than for the $dPL_{20(N)}$ case, with similar data dispersion). The value of these differences decreases from N=3 to N=1, as expected, due to the reduced ΔI currents between the "on" and "off" states as the number of isolated panels decreases. The SNR_{avg} values are 3.3, 4.4, and 2.1 for N=3, 2, and 1, respectively. It is observed that the ${\rm SNR}_{\rm avg}$ increases for the $dPL_{16(2)}$ case with respect to the $dPL_{16(3)}$ case, which can be attributed to the large ΔI current between the "on" and "off" states for the dPL₁₆₍₂₎ case (see Figures 9a,b), which is due to the large fluctuation of the irradiance for this set of measurements.

ON-OFF Signal (counts)

It is noticeable that the $\rm SNR_{avg}$ values of the different dEL/dPL images agree well with the mean value of the ON—OFF signal differences (which mainly correspond to the numerator of the expression in Equation (3)), the dispersion in the data (which mainly correspond to the denominator of the expression in Equation (3)), and the way the data are grouped around the mean value.

In this case (16/N), for all the measurements, we did not observe the changes over time in the minimum current intensity that were observed in the 20/5, 20/4, and 20/3 cases. This is likely due to the fact that the optimum operating voltage of the inverter for $S\!=\!16~(16\!\times\!V_{MPP}\!=\!16\!\times\!37.1\!=\!594.6\,V)$ is very close to its minimum operating voltage (560 V), and the efforts of the MPPT to maximize power during the switching measurement process produced almost no change.

3.2.3 | Inverter 2

As mentioned above, the response of the inverter to our $dPL_{S(N)}$ method for PV substrings during operation with electrical

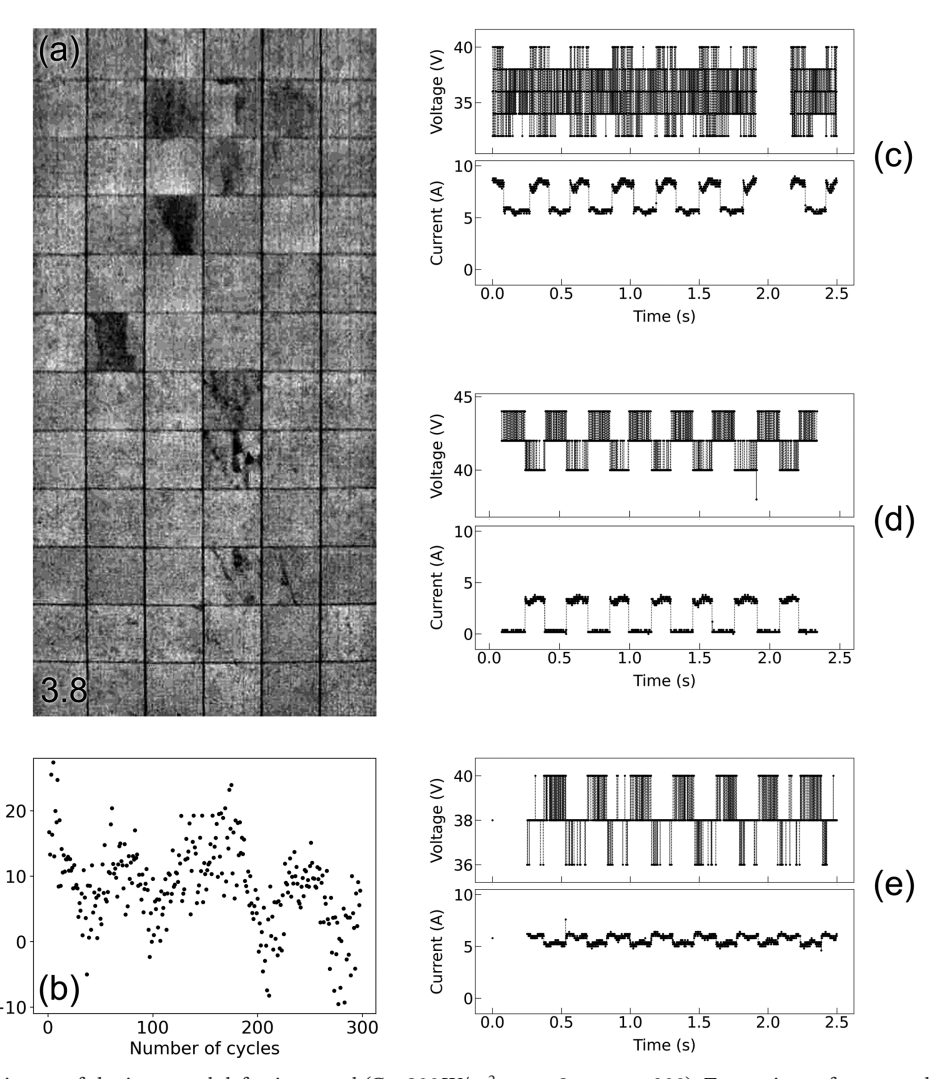


FIGURE 12 | (a) dPL_s image of the inspected defective panel ($G=800 \, \text{W/m}^2$, $t_{\text{exp}}=8 \, \text{ms}$, nc=300). Two strings of one panel each are connected to a microinverter; (b) ON—OFF signal differences, as a function of the number of cycles; (c–e) voltage and current intensity values, measured at the microinverter (c), at the terminals of the inspected panel (string#1) (d), and at the terminals of the parallel panel (string#2) (e) (only the first few seconds of the measurement are displayed).

modulation is dependent on the specific inverter model. To highlight this fact, another inverter INV2 was also tested to obtain the $dPL_{S(N)}$ measurements, both for the entire string of S = 20 panels as well as for a string of S = 16 panels. Figures 10 and 11 show the $dPL_{S(N)}$ images obtained $(G=1100 \text{ W/m}^2,$ nc = 300, $t_{exp} = 5$ ms) as well as the ON-OFF signal differences as a function of the number of cycles and the measured current and voltage values at the output of the inverter, for the cases S = 20, N = 6 (Figure 10), and S = 16, N = 3 (Figure 11). It can be seen that the response of the inverter to the switching process is quite different in this case compared to INV1. This should be ascribed to the presence of capacitors and the corresponding discharge processes. In any case—and despite the rather irregular shape of the current intensity waveform—the dPL_{S(N)} images obtained are still good enough to clearly observe almost the same defective cells as with INV1, especially in the 20/6 case. In fact, the $\mathrm{SNR}_{\mathrm{avg}}$ values are 8.1 and 5.2 for the 20/6 and 16/3 cases, respectively.

3.2.4 | Inspection of Whole Strings

The proposed procedure for inspecting substrings during operation can also be used for inspecting whole strings, as explained above (dPL_s). In order to test this methodology, and as a first attempt to validate it, we tested the case of two strings of just one panel (S=1) connected to a microinverter, with one of the panels being the defective panel shown in the previous figures. In this case, the electronic device was connected in series with the 1-panel string (see Figure 1b). Figure 12a,b shows the dPLs image for the case $G = 800 \text{ W/m}^2$, nc = 300, $t_{exp} = 8 \text{ ms}$, as well as the ON-OFF signal differences as a function of the number of cycles. Figure 12c-e shows the measured current and voltage values at the output of the inverter (c), in the inspected panel (string#1) (d) and in the parallel panel (string#2) (e). As can be seen, an almost perfect square wave modulation is again obtained for the current intensity drawn from the inspected panel (string#1) (Figure 12d). The maximum values of the current

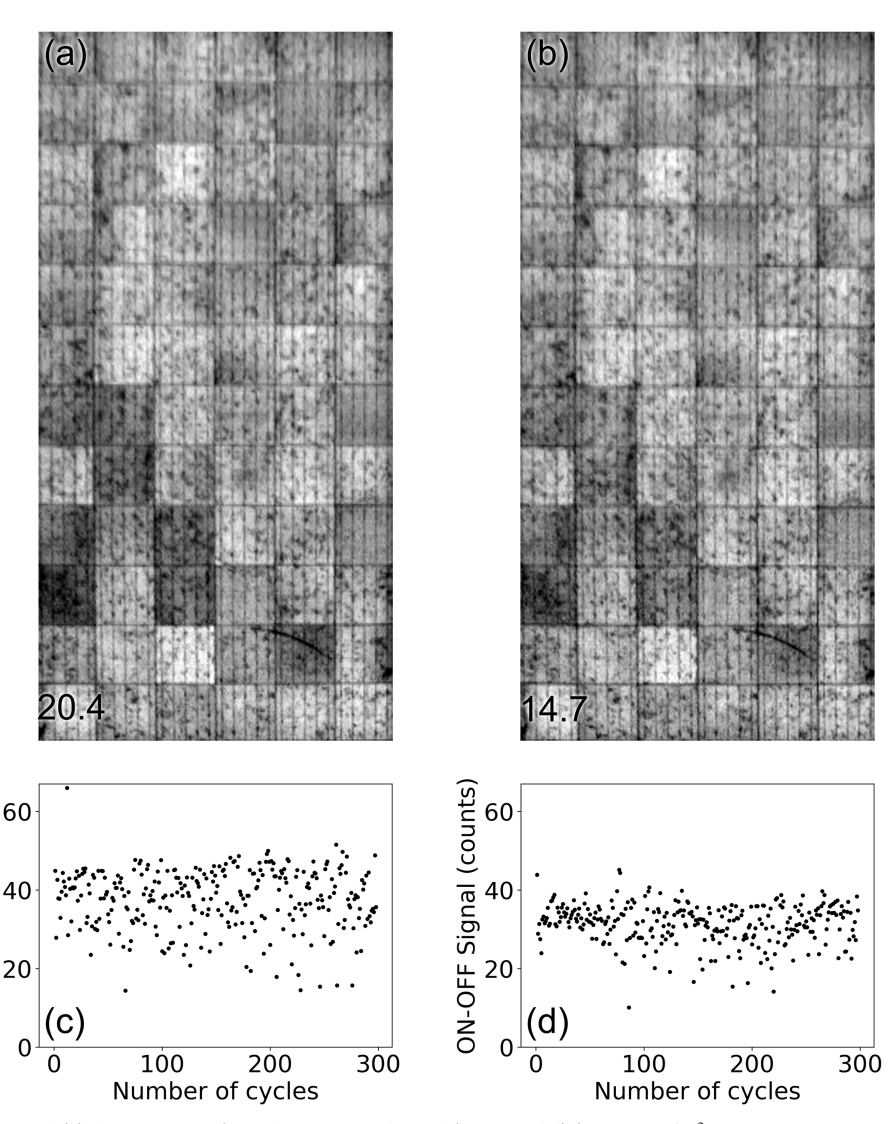


FIGURE 13 | (a) $dPL_{OC/SC}$ and (b) dPL_S images of another inspected panel (GCL model) (G=900 W/m², t_{exp} = 7 ms, nc = 300) (c,d) ON—OFF signal differences, as a function of the number of cycles, corresponding to the $dPL_{OC/SC}$ and dPL_S images, respectively.

ON-OFF Signal (counts)

intensity ("off" periods) are constant (~4.5 A) (corresponding to the irradiance value of the measurement) and the minimum values of the current intensity ("on" periods) are constant and equal to 0. The SNR_{avg} in this case is 3.8 (in good agreement with the large dispersion of the ON-OFF signal differences). Despite the low image quality, we can still distinguish the defective cells. It is also interesting to note that this dPL_s image provides slightly different information about the defects in the cells. The dPL_s information is more similar to the dEL image (Figure 3a) with regard to the $\mathrm{dPL}_{\mathrm{OC/SC}}$ image (Figure 4a). This result is currently unclear. It could be aligned with the previous comment on the information provided by dPL, depending on the current drawn from the PV panels in the "on" and "off" states, where the possibility of distinguishing a region's degree of isolation on a single dPL image was seen to depend on the level of current extraction and on the region's degree of isolation [26, 35]. This fact is now being studied in more detail.

Finally, Figure 13a,b shows the $dPL_{OC/SC}$ and dPL_S images obtained on a different panel (GCL model). Again, two strings of only one panel each (S=1) were connected to a microinverter. As can be seen, the dPL_S image is totally similar to the $dPL_{OC/SC}$ image, thus allowing the defects present in the different cells of the panels to be clearly distinguished. Material inhomogeneities, a large crack on a cell and cell inhomogeneities are well observed. (In this case, the information provided by dPL is almost the same as that obtained by dEL, see Figure S3.) Figure 13c,d shows the ON–OFF signal differences as a function of the number of cycles corresponding to the $dPL_{OC/SC}$ and dPL_S images, respectively. SNR_{avg} values of 20.4 and 14.7 are obtained, respectively, indicating a high quality of both images.

It should be noted that the ${\rm SNR}_{\rm avg}$ values are not fully comparable between different sets of measurements. Some anomalies with the ${\rm SNR}_{\rm avg}$ values have also been observed by other authors [31]. In our case, it is likely that the ${\rm SNR}_{\rm avg}$ value is influenced by several measurement parameters, including how well the PV panel is centered and positioned relative to the optical image captured (and how well the full resolution of the InGaAs camera is used). We are currently investigating this point in more detail.

The demonstration carried out with the microinverter merely seeks to validate the capability of the $\rm dPL_S$ procedure to inspect whole strings in operation. Current work on this topic with larger strings and PV plants is now in progress and will be published soon, together with the resemblance of the $\rm dPL_S$ measurements to the dEL images.

4 | Conclusions

The daylight photoluminescence (dPL) technique, which has recently emerged as a useful tool for inspecting solar panels on-site, has the advantage of not requiring an electrical power source, although a switching between two states is still generally necessary to filter the ambient light. Here, we describe a dPL procedure using an electronic device connected to a string (dPL $_{\rm S}$) or substring (dPL $_{\rm S(N)}$) to switch between two states with different currents drawn from the panels. The main idea is to carry out the inspection with the string in operation,

which makes it easier to monitor the condition of the panels throughout the life of the installation. The method allows the state of the string to be switched in a very fast and noninvasive manner, between the maximum power point state and a state at (or very close to) open circuit conditions. dPL_{S(N)} measurements were performed on a substring of 20-N or 16-N panels, testing the influence of the number of disconnected panels (N) from the string, and the response of two different inverters. The changes in the current intensity and voltage values at the output of the inverter and the quality of the $dPL_{S(N)}$ images obtained were correlated. Six panels or three panels were the optimum number of panels to be disconnected for the cases of 20 or 16 panels in the string, respectively. These are figures that depend on the characteristics of the panels (V_{OC}, V_{MPP}) and on those of the inverter. In those cases, a perfect square modulation of the current drawn from the panels was observed, between I_{MPP} and 0, with no effects by the self-readjustement of the MPPT of the inverter to increase the maximum power. The effect of capacitors was clearly observed for one of the tested inverters, modifying the square shape of the current drawn from the panels, although the $dPL_{S(N)}$ image obtained was still of sufficient quality. The procedure can be implemented to inspect whole strings, for which a demonstration using a microinverter capable of working with two panels in parallel was carried out. The $dPL_{S(N)}/dPL_S$ measurements obtained using this procedure were compared with conventional dPL measurements and dEL measurements. In particular, for the case of the microinverter, a dPLs image resembling the dEL image was observed, which could be ascribed to the two operating points selected for the "on" and "off" states, although this needs to be studied in more detail.

Author Contributions

Conceptualization: C. Terrados and O. Martínez. Software: D. González-Francés. Electronic design: C. Terrados and D. González-Francés. Measurement process: C. Terrados, D. González-Francés, K. P. Sulca, C. de Castro and O. Martínez. Data treatment: C. Terrados, D. González-Francés, K. P. Sulca and C. de Castro. Writing – original draft: C. de Castro, M. A. González and O. Martínez. Writing – review and editing: K. P. Sulca, M. A. González and O. Martínez. Supervision: O. Martínez.

Acknowledgments

This work has been financed by the Spanish Ministry of Science and Innovation, under projects PID2020-113533RB-C33 and PID2023-148369OB-C43 and by the Regional Government of Castilla y León (*Junta de Castilla y León*) and by the Ministry of Science and Innovation MICIN and the European Union NextGenerationEU/PRTR ("Plan Complementario de Materiales Avanzados en Castilla y León"). K. Sulca has been funded under the call for predoctoral contracts UVa 2022, co-financed by Banco Santander. C. de Castro is grateful for the funding from the *Programa Investigo* of the Spanish Ministry of Labour and Social Economy.

Data Availability Statement

The data that support the findings of this study are openly available in Zenodo at https://zenodo.org/records/15376094, reference number 15376094.

References

1. IEA-PVPS Trends Report 2023.

- 2. C. Ballif, F. J. Haug, M. Boccard, P. J. Verlinden, and G. Hahn, "Status and Perspectives of Crystalline Silicon Photovoltaics in Research and Industry," *Nature Reviews Materials* 7 (2022): 597–616.
- 3. IRENA. *Renewable Power Generation Costs in 2022* (International Renewable Energy Agency, 2022).
- 4. W. Muehleisen, G. C. Eder, Y. Voronko, et al., "Outdoor Detection and Visualization of Hailstorm Damages of Photovoltaic Plants," *Renewable Energy* 118 (2018): 138–145.
- 5. M. Aghaei, A. Fairbrother, A. Gok, et al., "Review of Degradation and Failure Phenomena in Photovoltaic Modules," *Renewable and Sustainable Energy Reviews* 159 (2022): 112160.
- 6. L. Koester, S. Lindig, A. Louwen, A. Astigarraga, G. Manzolini, and D. Moser, "Review of Photovoltaic Module Degradation, Field Inspection Techniques and Techno-Economic Assessment," *Renewable and Sustainable Energy Reviews* 165 (2022): 112616.
- 7. C. Del Pero, N. Aste, F. Leonforte, and F. Sfolcini, "Long-Term Reliability of Photovoltaic c-Si Modules—A Detailed Assessment Based on the First Italian BIPV Project," *Solar Energy* 264 (2023): 112074.
- 8. S. Gallardo-Saavedra, L. Hernández-Callejo, M. C. Alonso-García, et al., "Nondestructive Characterization of Solar PV Cells Defects by Means of Electroluminescence, Infrared Thermography, I-V Curves and Visual Tests: Experimental Study and Comparison," *Energy* 205 (2020): 117930.
- 9. I. Høiaas, K. Grujic, A. Gerd, I. Burud, E. Olsen, and N. Belbachir, "Inspection and Condition Monitoring of Large-Scale Photovoltaic Power Plants: A Review of Imaging Technologies," *Renewable and Sustainable Energy Reviews* 161 (2022): 112353.
- 10. M. W. Akram, G. Li, Y. Jin, and X. Chen, "Failures of Photovoltaic Modules and Their Detection: A Review," *Applied Energy* 313 (2022): 118822.
- 11. G. Tanda and M. Migliazzi, "Infrared Thermography Monitoring of Solar Photovoltaic Systems: A Comparison Between UAV and Aircraft Remote Sensing Platforms Thermal Science and Engineering Progress," *Thermal Science and Engineering Progress* 48 (2024): 102379.
- 12. M. Köntges, S. Kurtz, C. Packard, et al., *IEA-PVPS Task 13: Performance and Reliability of Photovoltaic Systems. Subtask 3.2: Review of Failures of Photovoltaic Modules.* Technical report, (International Energy Agency, 2014).
- 13. M. Navarrete, L. Pérez, F. Domínguez, et al., "On-Site Inspection of PV Modules Using an Internationally Accredited PV Mobile Lab: A Three-Year Experience Operating Worldwide," in 31st European Photovoltaic Solar Energy Conference and Exhibition (EUPVSEC, 2015): 1989.
- 14. O. Kunz, J. Schlipf, A. Fladung, et al., "Outdoor Luminescence Imaging of Field-Deployed PVmodules Prog," *Energy* 4 (2022): 042014.
- 15. M. Demant, J. Haunschild, M. Glatthaar, et al., "Quality Control of As-Cut Multicrystalline Silicon Wafers Using Photoluminescence Imaging for Solar Cell Production," *Solar Energy Materials and Solar Cells* 94 (2010): 2007.
- 16. B. Doll, J. Hepp, M. Hoffmann, et al., "Photoluminescence for Defect Detection on Full-Sized Photovoltaic Modules," *IEEE Journal of Photovolt.* 11 (2021): 1419.
- 17. NREL A Faster, Cheaper Way to Give Solar Panels a Clean Bill of Health. 2023. (Accessed 17 January 2025 https://www.nrel.gov/news/program/2023/a-faster-cheaper-way-to-give-solar-panels-a-clean-bill-of-health.html).
- 18. G. A. dos Reis Benatto, C. Mantely, A. A. Santamaria Lancia, P. B. Poulsen, S. Forchhammery, and S. V. Spataru, "Laser Induced Luminescence Characterization of Mechanically Stressed PV Cells," in *Proceedings of 48th IEEE Photovoltaic Specialists Conference* (IEEE, 2021): 1949–1953.

- 19. L. Stoicescu, M. Reuter, and J. H. Werner, "Daysy: Luminescence Imaging of PV Modules in Daylight," in 29th European Photovoltaic Solar Energy Conference and Exhibition (EUPVSEC, 2014): 2553.
- 20. J. Adams, B. Doll, C. Buerhop, et al., "Non-Stationary Outdoor EL-Measurements With a Fast and Highly Sensitive InGaAs Camera," in 32nd Eur. Photovolt. Sol. Energy Conf. Exhib (EUPVSEC, 2015): 1837.
- 21. S. Koch, T. Weber, C. Sobottka, A. Fladung, P. Clemens, and J. Berghold, "Outdoor Electroluminescence Imaging of Crystalline Photovoltaic Modules: Comparative Study Between Manual Ground Level Inspections and Drone-Based Aerial Surveys," in *32nd European Photovoltaic Solar Energy Conference and Exhibition* (2016): 1736.
- 22. G. A. dos Reis Benatto, N. Riedel, S. Thorsteinsson, et al., "Development of Outdoor Luminescence Imaging for Drone-Based Pv Array Inspection," in *Proc. 44th IEEE Photovolt. Specialist Conf.* (IEEE, 2017): 2682–2687.
- 23. M. Guada, A. Moretón, S. Rodríguez-Conde, et al., "Daylight Luminescence System for Silicon Solar Panels Based on a Bias Switching Method," *Energy Science & Engineering* 8 (2020): 3839.
- 24. R. Bhoopathy, O. Kunz, M. Juhl, T. Trupke, and Z. Hameiri, "Outdoor Photoluminescence Imaging of Photovoltaic Modules With Sunlight Excitation," *Progress in Photovoltaics: Research and Applications* 26 (2018): 69.
- 25. L. Koester, A. Louwen, S. Lindig, G. Manzolini, and D. Moser, "Large-Scale Daylight Photoluminescence: Automated Photovoltaic Module Operating Point Detection and Performance Loss Assessment by Quantitative Signal Analysis," *Solar RRL* 8 (2024): 2300676.
- 26. M. Vuković, M. S. Wiig, G. A. dos Reis Benatto, E. Olsen, and I. Burud, "A Review of Imaging Methods for Detection of Photoluminescence in Field-Installed Photovoltaic Modules," *Progress in Energy* 6 (2024): 032001.
- 27. H. Herrmann, G. Eder, B. Farnung, et al., Qualification of Photovoltaic PV Power Plants Using Mobile Test Equipment IEA-PVPS T13-24 (International Energy Agency (IEA), 2021): 2021.
- 28. O. Kunz, G. Rey, M. K. Juhl, and T. Trupke, "High Throughput Outdoor Photoluminescence Imaging via PV String Modulation," in *IEEE 48th Photovoltaic Specialists Conference (PVSC)*, vol. 2021 (IEEE, 2021): 346–350.
- 29. O. Kunz, J. W. Weber, G. Rey, M. Juhl, and T. Trupke, "Daylight Photoluminescence Imaging via Optical String Switching," *Solar RRL* 8 (2024): 2400385.
- 30. M. Vuković, M. Jakovljevic, A. S. Flø, E. Olsen, and I. Burud, "Non-invasive Photoluminescence Imaging of Silicon PV Modules in Daylight," *Applied Physics Letters* 120 (2022): 244102.
- 31. J. W. Weber, O. Kunz, C. Knaack, et al., "Daylight Photoluminescence Imaging of Photovoltaic Systems Using Inverter-Based Switching," *Progress in Photovoltaics: Research and Applications* 32 (2024): 643.
- 32. M. Vuković, I. E. Høiaas, M. Jakovljevic, A. S. Flø, E. Olsen, and I. Burud, "Photoluminescence Imaging of Silicon Modules in a String," *Progress in Photovoltaics: Research and Applications* 30 (2022): 436–446.
- 33. G. A. dos Reis Benatto, R. del Prado-Santamaría, S. V. Spataru, et al., "Image Quality Evaluation of Contactless Outdoor Photoluminescence Based on String Inverter's IV Curve Sweep Capability," in 40th European Photovoltaic Solar Energy Conference and Exhibition, 020383-001-005 (EU PVSEC, 2023).
- 34. O. Kunz, G. Rey, R. Bhoopathy, Z. Hameiri, and T. Trupke, "Outdoor PL Imaging of Crystalline Silicon Modules at Constant Operating Point," in *47th IEEE Photovoltaic Specialists Conf. (PVSC)* (IEEE, 2020): 2140–2143.
- 35. G. Rey, O. Kunz, M. Green, and T. Trupke, "Luminescence Imaging of Solar Modules in Full Sunlight Using Ultranarrow Bandpass

Filters," Progress in Photovoltaics: Research and Applications 30 (2022): 1115–1121.

- 36. IEC TS 60904–13, "Photovoltaic Devices—Part 13: Electroluminescence of Photovoltaic Modules" (2018).
- 37. C. Mantel, G. A. dos Reis Benatto, N. Riedel, et al., "SNR Study of Outdoor Electroluminescence Images Under High Sun Irradiation," in *Proc. IEEE 7th World Conf. Photovolt. Energy Convers* (IEEE, 2018): 3285–3289.
- 38. C. Terrados, D. González-Francés, V. Alonso, M. A. González, J. Jiménez, and O. Martínez, "Comparison of Outdoor and Indoor PL and EL Images in Si Solar Cells and Panels for Defect Detection and Classifcation," *Journal of Electronic Materials* 52 (2023): 5189–5198.
- 39. M. Vuković, *Toward Monitoring of Photovoltaic Power Plants With Photoluminescence Imaging*. PhD Thesis (Norwegian University of Life Sciences, 2023).
- 40. C. Terrados, D. González-Francés, J. Anaya, et al., "Improvements in the Acquisition of Daylight Electroluminescence Images Using High Speed Cameras: Comparison of Square and Sinusoidal Waves Excitations," in 40th Eur. Photovolt. Sol. Energy Conf. Exhib (EUPVSEC, 2023) 2023, 3DO.16.5.

Supporting Information

Additional supporting information can be found online in the Supporting Information section.